Journal of Ceramic Processing Research. Vol. 17, No. 10, pp. 1015~1018 (2016)

JOURNAL OF
Ceramic
Processing Research

# Defect reduction in m-plane GaN on m-sapphire via lateral epitaxial overgrowth by hydride vapor phase epitaxy

**Minho Kim[a], Seohwi Woo[a], Byeongchan So[a], Kwang Bo Shim[b] and Okhyun Nam[a,*]**

[a]*Convergence Center for Advanced Nano Semiconductor (CANS), Department of Nano-Optical Engineering, Korea Polytechnic University (KPU),237, Sangidaehak-ro, Siheung-si, Gyeonggi-do, 429-793, Korea*

[b]*Division of Materials Science and Engineering, Hanyang University, 17 Hangdang-dong Seongdong-gu, Seoul 133-791, Korea*

**We report on the improvement of the structural and optical properties of *m*-plane GaN layers on *m*-plane sapphire via epitaxial lateral overgrowth (ELO) using hydride vapor phase epitaxy. The planar *m*-plane GaN was compared to ELO *m*-plane GaN with stripes patterned along the [11$\bar{2}$0] and [0001], respectively. The ELO *m*-plane GaN samples showed narrow x-ray rocking curves and more improved cathodoluminescence (CL) images compared with those of the planar *m*-plane GaN. The density of threading dislocations (TDs) and basal-plane stacking faults (BSFs) was decreased in the ELO *m*-plane GaN, which was confirmed by transmission electron microscopy (TEM) and Williamson - Hall (W-H) plot analysis.**

**Keywords: HVPE, *m*-plane GaN, ELO, m-plane sapphire.**

## Introeduction

GaN-based optoelectronic devices have enabled high-efficiency, high-power light-emitting diodes (LEDs) in the ultra-violet to visible spectrum and high-power electronic devices. Commercial GaN-based LEDs are grown on the *c*-plane of a hexagonal wurtzite structure. However, conventional *c*-plane GaN suffers from the quantum-confined Stark effect (QCSE) because of the existence of strong piezoelectric and spontaneous polarization. These polarization fields cause spatial separation of electrons and holes in quantum-well structures and reduce the overlap of the electron-hole wave functions, which leads to reduced optical emission efficiency [1, 2]. To solve this problem, many research groups have focused on the growth of non-polar GaN layers, for example (11$\bar{2}$0) [3] and (10$\bar{1}$0) [4], and semi-polar layers, for example (11$\bar{2}$2) [5], (10$\bar{1}$3) [6], and (20$\bar{2}$1) [7]. In particular, non-polar layers exhibit no internal polarization fields along the growth direction. This is advantageous for fabrication of optoelectronic devices with high performance. In the case of *m*-plane GaN, it has been grown on substrates such as *m*-plane SiC [4], $LiAlO_2$ [8], *m*-plane ZnO [11], m-sapphire [10, 11, 12], and patterned *a*-sapphire [13]. Among these substrates, it was found that *m*-sapphire was more stable than $LaAlO_3$ and ZnO [14]. Therefore, recently, many groups have studied *m*-plane GaN growth on *m*-sapphire. However, *m*-plane GaN still suffers from reduced crystalline quality as compared to conventional *c*-plane GaN, showing higher density of structural defects, basal-plane stacking faults (BSFs) and threading dislocations (TDs). These defects usually act as non-radiative centers, significantly affecting the optical and electrical properties and reliabilities of LED devices, especially under high-current conditions.

In this paper, we have investigated improved *m*-plane GaN on *m*-plane sapphire via epitaxial lateral overgrowth (ELO) using hydride vapor-phase epitaxy (HVPE) in terms of defect reduction according to stripe direction.

## Experimental

The HVPE growth process was carried out in a vertical hot-wall quartz reactor. The reactor was divided into two temperature zones, the source zone and the growth zone. Ga, HCl, and $NH_3$ were used as the sources gases and $N_2$ served as the carrier gas. The *m*-plane GaN layers were grown on *m*-plane sapphire substrates at a growth temperature of 1040 $^{o}$C. Prior to the process, the sapphire substrates were heated for 5 min in order to ensure thermal stabilization. Growth began without any initial treatment, such as $H_2$ cleaning or nitridation, because growth of GaN films on the *m*-sapphire is changed by initial growth conditions. [11, 12]. The 100-nm-thick $SiO_2$ films were deposited on *m*-plane GaN templates using a plasma-enhanced chemical-vapor deposition (PECVD) system. ELO patterns consisting of 3 μm-wide $SiO_2$ stripes and 3 μm-wide GaN windows were generated using conventional photolithography processes. The $SiO_2$ stripes were formed along [11$\bar{2}$0] and [0001] on the GaN layer. Next, approximately 15 μm of *m*-plane GaN was

*Corresponding author:
Tel : +82-31-8041-1916
Fax: +82-31-8041-1917
E-mail: ohnam@kpu.ac.kr

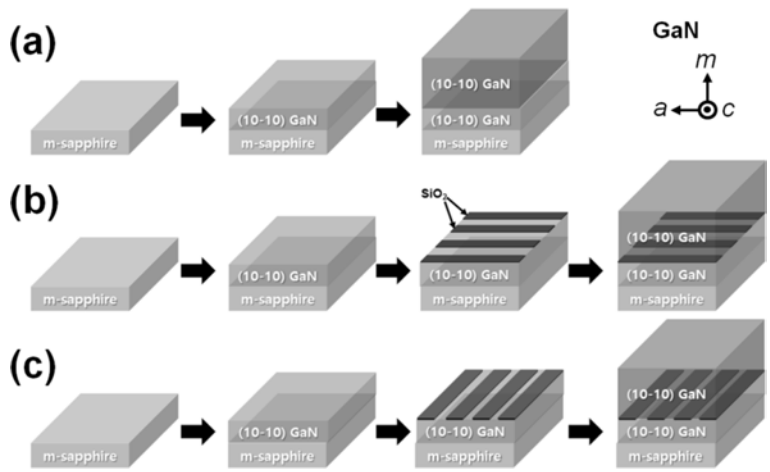


**Fig. 1.** Schematic images of experimental procedure of (a) planar, (b) [11-20] stripes, and (c) [0001] stripes.

regrown by HVPE. Fig. 1 shows a schematic of the experimental process.

The surface morphology of the $m$-plane GaN layer was observed using scanning electron microscopy (SEM). The crystal quality of the GaN layer was measured using an omega scan of double-crystal X-ray diffraction (DCXRD). A CL analysis was performed in order to investigate the luminescence properties of the $m$-plane GaN layer. The plane view of the $m$-plane GaN defects was observed by TEM.

## Results and Discussion

Fig. 2 shows the cross-sectional SEM images of planar and ELO samples. All samples are fully merged. After complete coalescence, periodic triangular cavities were formed in [0001] stripe-patterned $m$-plane GaN. The inset images show anisotropy of the growth rate at sample (b) and (c). Epitaxial relationship with $m$-plane GaN on $m$-sapphire is oriented a 90 $^{o}$ in-plane rotation giving the following epitaxial relationships: $[0001]_{GaN}$ | | $[11\bar{2}0]_{sap}$ and $[11\bar{2}0]_{GaN}$ | | $[0001]_{sap}$ [11]. Therefore, the $[11\bar{2}0]$ stripes have overgrown along the $c$-axis. The growth rate on the Ga face (+ $c$-direction) was approximately five times higher than on the N-face ($-c$-direction). This growth-rate change is due to the differing conditions, i.e., V/III ratio, temperature, and pressure [15]. The [0001] stripes on the sample have overgrown along the $a$-axis, exhibiting five $m$-plane facets.

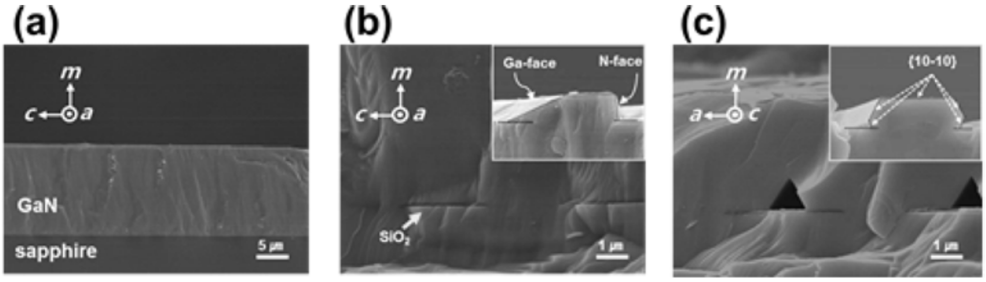


**Fig. 2.** Cross-sectional SEM images of (a) planar, (b) [11-20] stripes, and (c) [0001] stripes. The inset images show anisotropy of growth rate.

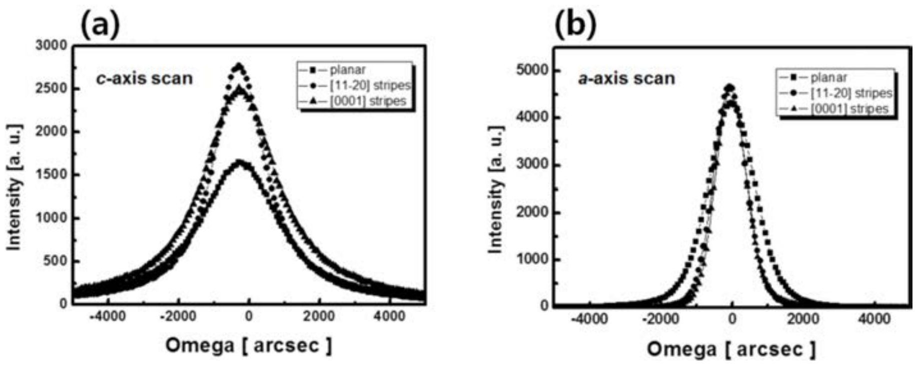


**Fig. 3.** X-ray rocking curves of the (10-10) reflection of $m$-plane GaN layer grown on the planar, [11-20], [0001] stripes pattern. (a) and (b) correspond to diffraction along the parallel and vertical direction to the $c$-axis, respectively.

Fig. 3 shows the FWHM of the X-ray rocking curves (XRCs) for the on-axis diffraction planes. The FWHMs for the $(10\bar{1}0)$ plane along the [0001] and $[11\bar{2}0]$ direction scans for the planar sample were 2660 and 1360 arcsec, respectively. The FWHMs for the $[11\bar{2}0]$ stripe sample were 1670 and 1110 arcsec, and for the [0001] stripe sample were 2600 and 1030 arcsec, respectively. These FWHM results indicate that the ELO samples are narrower than the planar samples because defects such as TD and BSF are blocked by the $SiO_2$ mask. All the FWHMs are broader in the [0001] direction scan compared to the $[11\bar{2}0]$, which is because many structural defects were introduced along this direction [16].

Fig. 4 shows the modified Williamson-Hall (W-H) plots of the FWHM from the (n0n0) series of the *m*-plane GaN layers, inS which the scan was parallel to the [0001] direction. According to the previous reports, the (n0-n0) XRCs FWHM results correlate with the density of BSFs [17, 18]. W-H plot analysis can be performed, noting [FWHM × sin(θ)/λ] on the y-axis and [sin(θ)/λ] on the x-axis. From the y-intersection $y_0$ of the fitted line, the lateral coherence length (LCL) can be estimated [19],

$$\mathrm{LCL} = \frac{0.9}{(2y_0)} \qquad (1)$$

The reciprocal of the LCLs gives the density of BSFs. The determined BSF density of planar, $[11\bar{2}0]$ stripes, and [0001] stripes were $2.0 \times 10^5\,\mathrm{cm}^{-1}$, $5.0 \times 10^4\,\mathrm{cm}^{-1}$, and $1.0 \times 10^5\,\mathrm{cm}^{-1}$, respectively. These results correspond with the plane-view TEM images in Fig. 5. The $(30\bar{3}0)$ value was smaller than other planes. Because of $(30\bar{3}0)$ reflection was not affected by BSFs but may indicate possible surface roughness-related effects [18].

Fig. 6 shows a monochromatic CL surface image. The bright fields correspond to defect-free regions and dark spots correspond to no-luminescence regions, which are attributed to dislocations functioning as non-radiative centers [20]. The wing region of the ELO samples exhibits increased luminescence intensity compared with the window region and planar sample. Radiation of the dislocations was more sensitive than BSFs in the CL analysis. Therefore, the brightnesses of the $[11\bar{2}0]$ stripes and [0001] stripes were similar, although the BSF densities were different. The black lines at the center of the wing region at the $[11\bar{2}0]$ and [0001] stripe patterns are coalescence boundaries, in which threading dislocations were generated [21].

Fig. 5 shows a plane-view TEM image of the ELO samples. Figs. 5(a) and 5(c) were imaged under the $g = 0002$ diffraction condition and (b) and (d) were imaged under the $g = 11\bar{2}0$ diffraction condition, which reveal

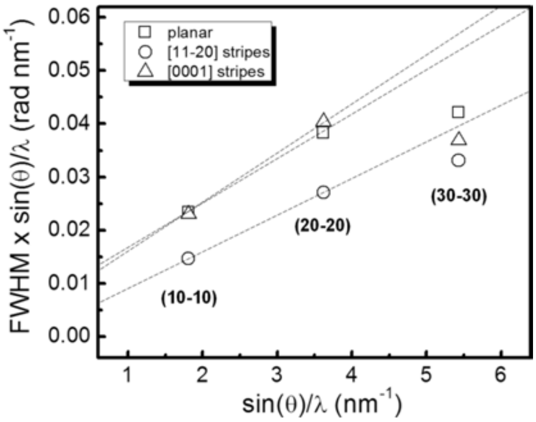


**Fig. 4.** Williamson-Hall plots of FWHM from the (n0-n0) series of reflections for planar, [11-20] stripes, and [0001] stripes.

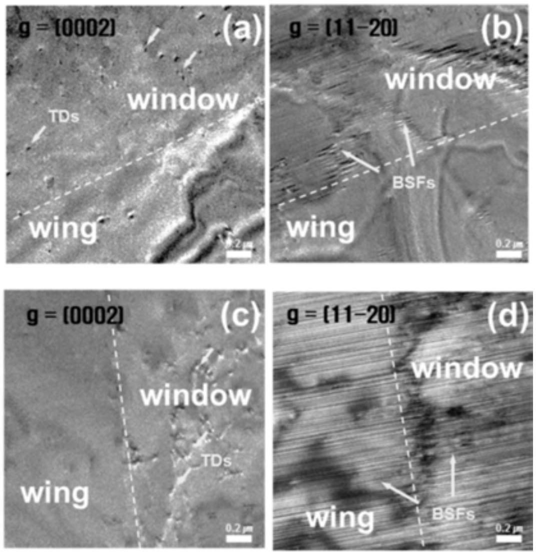


**Fig. 5.** Plane-view TEM images of *m*-plane GaN, (a) and (b) : [11-20] stripes, (c) and (d) : [0001] stripes.

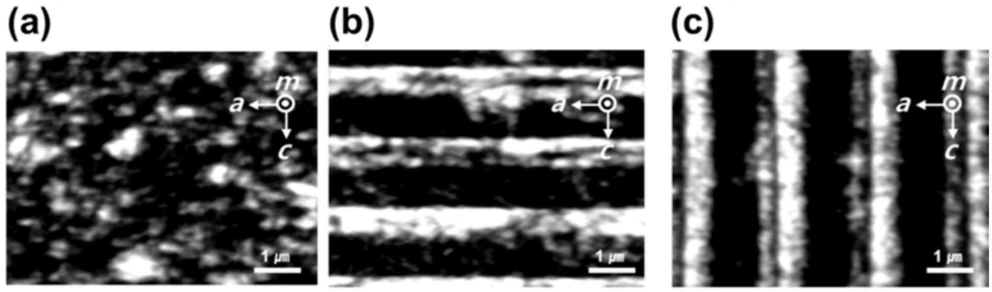


**Fig. 6.** Room-temperature monochromatic CL images of (a) planar, (b) [11-20] stripes, and (c) [0001] stripes.

TDs and BSFs, respectively [22, 23]. The TD densities of the [11$\bar{2}$0] stripe-patterned *m*-plane GaN on the wing and window regions are $4 \times 10^8$ and $5 \times 10^{10}$ cm$^{-2}$, respectively. The BSF densities measured for the layers grown on the wing and window regions are $3 \times 10^4$ and $4 \times 10^5$ cm$^{-1}$, respectively. And, TD densities of the [0001] stripe-patterned *m*-plane GaN on the wing and window regions are $3.6 \times 10^8$ and $6.0 \times 10^{10}$ cm$^{-2}$, respectively. The BSF densities measured for the layers grown on the wing and window regions were the same: $4 \times 10^5$ cm$^{-1}$. TD densities have dramatically decreased in the wing region. However, in terms of BSF densities, only [11$\bar{2}$0] stripes are one order of magnitude lower than other samples.

## Conclusions

We have successfully grown *m*-plane GaN on *m*-plane sapphire by HVPE. XRC FWHMs of ELO samples were improved for both [11$\bar{2}$0] stripes and [0001] stripes, and CL intensity also was increased in the wing regions. The TD and BSF densities of the [11$\bar{2}$0] stripes on the wing and window regions were $4 \times 10^8$ and $5 \times 10^{10}$ cm$^{-2}$, and $3 \times 10^4$ and $4 \times 10^5$ cm$^{-1}$, respectively. The TD and BSF densities of the [0001] stripes on the wing and window regions were $3.6 \times 10^8$ and $6.0 \times 10^{10}$ cm$^{-2}$, and $4 \times 10^5$ cm$^{-1}$. In the case of TD density, the decreasing rate was the same for both stripes, but the BSF density decreased only for [11$\bar{2}$0] stripes. The TEM results also corresponded with the analysis of the W-H plot.

## Acknowledgments

This work was supported by Industrial Strategic Technology Development Program of the Ministry of Trade, industry and Energy (no. 10041188) and by the National Research Foundation of Korea (NRF) grant funded by the Korea government (MEST) No. 2012R1A2A2A01011702.

## Reference

1. O. Ambacher, R. Dimitrov, M. Stutzmann, B.E. Foutz, M.J. Murphy, J.A. Smart, J.R. Shealy, N.G. Weiman, K. Chu, M. Chumbes, B. Green, A.J. Sierakowski, W.J. Schaff, and L.F. Eastman: phys. stat. sol. (b) 216 (1999) 381.
2. M. B. Nardelli, K. Rapcewicz, and J. Bernholc : Appl. Phys. Lett. 71 (1997) 21.
3. Geunho Yoo, Hyunsung Park, Hyoungjin Lim, Seunga Lee, Okhyun Nam, Youngboo Moon, Chaerok Lim, Bohyun Kong, and Hyungkoun Cho: Jpn. J. Appl. Phys. 50 (2011) 042103.
4. Bilge IMER, Feng WU, Michael D. CRAVEN, James S. SPECK and Steven P. DENBAARS : Jpn. J. Appl. Phys 45 (2006) 8644-8647.
5. Jongjin Jang, Kwanhyun Lee, Junghwan Hwang , Joocheol Jung, Seunga Lee, Kyuho Lee, Bohyun Kong , Hyunghoun Cho , OkhyunNam : J. Cryst. Growth. 361 (2012) 166-170.
6. T.B.Wei, Q.Hu, R.F.Duan, X.C.Wei, Z.Q.Huo, J.X.Wang, Y.P.Zeng, G.H.Wang, J.M.Li : J. Cryst. Growth. 311 (2009) 4153-4157.
7. Narihito Okada, Hiroyasu Oshita, Keisuke Yamane, and Kazuyuki Tadatomo : Appl. Phys. Lett. 99 (2011) 242103.
8. P. Waltereit, O. Brandt, M. Ramsteiner, A. Trampert, H.T. Grahn, J. Menniger, M. Reiche, K.H. Ploog : J. Cryst. Growth. 227-228 (2011) 437-441.
9. Atsushi Kobayashi, Satoshi Kawano, Yuji Kawaguchi, Jitsuo Ohta, and Hiroshi Fujioka : Appl. Phys. Lett. 90 (2007) 041908.
10. Hyun-Jae Lee, K. Fujii, T. Goto, T. Yao, and Jiho Chang : Appl. Phys. Lett. 98 (2011) 071904.
11. Philippe Venngus, Tiankai Zhu, Denis Martin, and Nicolas Grandjean : J. Appl. Phys. 108 (2010) 113521.
12. Yeonwoo Seo, Sanghwa Lee, Miyeon Jue, Hansub Yoon, and Chinkyo Kim : Appl. Phys. Exp. 5 (2012) 121001 .
13. Narihito Okada, Yuji Kawashima, and Kazuyuki Tadatomo : Appl. Phys. Exp. 1 (2008) 111101.
14. J. Zoua, Y. Dongc, S. Zhoua, Y. Sund, W. Juna, J. Zhoua, T. Huanga , S. Yange, H. Zhoue, J. Cryst. Growth. 294 (2006) 339-342.
15. M. D. Craven, S. H. Lim, F. Wu, J. S. Speck, and S. P. DenBaars : Appl. Phys. Lett. 81 (2002) 1201-1203.
16. Hitoshi Sasaki, Haruo Sunakawa, Norihiko Sumi, Kazutomi Yamamoto, Akira Usui : J. Cryst. Growth. 311 (2009) 2910-2913.
17. \Melvin B. MCLAURIN, Asako HIRAI, Erin YOUNG, Feng WU, and James S. SPECK : Jpn. J. Appl. Phys. 47 (2008) 5429-5431.
18. M. A. Moram, C. F. Johnston, J. L. Hollander, M. J. Kappers, and C. J. Humphreys J. Appl. Phys. 105 (2009) 113501.
19. T. Metzger, R. Höpler, E. Born, O. Ambacher, M. Stutzmann, R. Stömmer, M. Schuster, H. Göbel, S. Christiansen, M. Albrecht & H. P. Strunk : Philos. Mag. A 77 (1998) 1013-1025.
20. Tomoya SUGAHARA, Hisao SATO, Maosheng HAO, Yoshiki NAOI, Satoshi KURAI, Satoru TOTTORI, Kenji YAMASHITA, Katsushi NISHINO, Linda T. ROMANO and Shiro SAKAI : Jpn. J. Appl. Phys. 37 (1998) pp. L398-L400.
21. P. Vennéguès, B. Beaumont, V. Bousquet, M. Vaille, and P. Gibart : J. Appl. Phys. 87 (2000) 4175.
22. Bo Hyun Kong, Qian Sun, Jung Han, In-Hwan Lee, Hyung Koun Cho : Appl. Surf. Sci. 258 (2012) 2522-2528.
23. Youngji Cho , Sungkuk Choi , Gyung-Suk Kil , Hyun-Jae Lee , Takafumi Yao , Jun-MoYang , Jungho Yoo , Jangwoo Kwone, Jiho Chang : 325 (2011) 85-88.